

CAE-TRANSFORMER: TRANSFORMER-BASED MODEL TO PREDICT INVASIVENESS OF LUNG ADENOCARCINOMA SUBSOLID NODULES FROM NON-THIN SECTION 3D CT SCANS

Shahin Heidarian[†], Parnian Afshar[‡], Anastasia Oikonomou, ^{††},
Konstantinos N. Plataniotis^{‡‡}, and Arash Mohammadi[‡]

[†]Department of Electrical and Computer Engineering, Concordia University, Montreal, Canada

[‡]Concordia Institute for Information Systems Engineering, Concordia University, Montreal, Canada

^{††}Department of Medical Imaging, Sunnybrook Health Sciences Centre, Toronto, Canada

^{‡‡}Department of Electrical and Computer Engineering, University of Toronto, Toronto, Canada

ABSTRACT

Lung cancer is the leading cause of mortality from cancer worldwide and has various histologic types, among which Lung Adenocarcinoma (LAUC) has recently been the most prevalent. Lung adenocarcinomas are classified as pre-invasive, minimally invasive, and invasive adenocarcinomas. Timely and accurate knowledge of the invasiveness of lung nodules leads to a proper treatment plan and reduces the risk of unnecessary or late surgeries. Currently, the primary imaging modality to assess and predict the invasiveness of LAUCs is the chest CT. The results based on CT images, however, are subjective and suffer from a low accuracy compared to the ground truth pathological reviews provided after surgical resections. In this paper, a predictive transformer-based framework, referred to as the "CAE-Transformer", is developed to classify LAUCs. The CAE-Transformer utilizes a Convolutional Auto-Encoder (CAE) to automatically extract informative features from CT slices, which are then fed to a modified transformer model to capture global inter-slice relations. Experimental results on our in-house dataset of 114 pathologically proven Sub-Solid Nodules (SSNs) demonstrate the superiority of the CAE-Transformer over the histogram/radiomics-based models and its deep learning-based counterparts, achieving an accuracy of 87.73%, sensitivity of 88.67%, specificity of 86.33%, and AUC of 0.913, using a 10-fold cross-validation.

Index Terms— Lung Adenocarcinoma, Lung Nodule Invasiveness, Transformer, Subsolid Nodule, Self-Attention.

1. INTRODUCTION

Lung Cancer (LC) is the deadliest and least funded cancer worldwide [1, 2]. Non-small-cell LC is the major type of LC, and Lung Adenocarcinoma (LUAC) is the most prevalent histologic subtype [3]. Lung nodules manifesting as Ground Glass (GG) or subsolid nodules on CT, have a higher risk of malignancy than other incidentally detected small solid nodules. Subsolid Nodules (SSNs) are often diagnosed as adenocarcinoma and are generally classified into pure GGNs (pGGNs) and part-solid nodules (PSNs) according to their appearance on the lung window settings [4, 5]. LUACs are categorized according to their histology into three categories: pre-invasive lesions including atypical adenomatous hyperplasia (AAH)

and adenocarcinoma in situ (AIS), minimally invasive (MIA), and invasive pulmonary adenocarcinoma (IPA) [5]. A timely and accurate attempt to differentiate the LUACs is of utmost importance to guide a proper treatment plan, as in some cases, a pre-invasive or minimally invasive SSN can be monitored with regular follow up CTs, whereas invasive lesions should undergo immediate surgical resection if they are deemed eligible. Most often, the SSN's types are diagnosed based on their pathological findings performed after surgical resections which is not desired for prior treatment planning. Currently, radiologists use chest Computed Tomography (CT) scans to assess the invasiveness of the SSNs based on their imaging findings and patterns prior to making decisions regarding the appropriate treatment. Such visual approaches, however, are time-consuming, subjective, and error-prone. So far, many studies have used high-resolution and thin-slice ($< 1.5mm$) CT images (slices) for the SSN classification, which require longer analysis times, as well as more storage capacity and reconstruction time [6, 7]. Recent lung cancer screening recommendation, however, suggests using Low Dose CT scans (LDCT) with thicker slice-thicknesses (up to $2.5mm$) [8, 9]. Moreover, lung nodules are mostly identified from CT scans performed for varied clinical purposes acquired using routine standard or low dose scanning protocols with non-thin slice thicknesses (up to $5mm$) [10]. Capitalizing on the above discussion, the necessity of developing an automated classification framework that performs well regardless of technical settings has recently arisen among the research community and healthcare professionals.

Related Works: In general, existing publications on the SSN classification and invasiveness assessment can be categorized into two main groups: (1) Radiomics-based and (2) Deep Learning-based frameworks [11]. In the former, a set of histogram-based, morphological, and clinical features are extracted from the CT images which are then analyzed using statistical or machine learning techniques such as the studies conducted in [12, 13]. As another example of such frameworks, a histogram-based model is developed in [10] to predict the invasiveness of primary adenocarcinoma SSNs from non-thin CT scans of 109 pathologically labeled SSNs. In this study, a set of histogram-based and morphological features along with additional features extracted via the Functional Principal Component Analysis (FPCA) is fed to a linear logistic regression, achieving the accuracy of 81.0% and Area Under the ROC Curve (AUC) of 0.91. Deep learning-based frameworks, on the other hand, extract informative and discriminative features in an automated fash-

This work was partially supported by the Natural Sciences and Engineering Research Council (NSERC) of Canada through the Create Grant RGPIN-2016-04988.

ion. Existing deep models working with volumetric CT scans can be classified into two main groups: (i) The first approach is to feed the whole volume of images (i.e., all 2D slices) or stack of all nodule patches (cropped images including nodules) into a 3D model (e.g., 3D CNN) to provide a patient-level prediction [14, 15]. Processing a large 3D CT scan at once, however, demands more complex models, more computational resources, and larger training datasets. (ii) The second approach, on the other hand, analyzes individual 2D CT slices or Regions of Interest (ROIs) in the first step and aggregate the results through a sequential model such as RNN or LSTM or via another aggregation mechanism based on pooling or fully connected layers [16, 17, 18]. It is also worth noting that most of the published studies are developed and evaluated based on the public LIDC-IDRI [19] dataset which does not have pathologically proven labels and focuses more on nodule detection than classification.

Due to the nature of the volumetric CT scans which utilize a sequence of 2D images (slices) to provide a detailed representation of the body, there have been recently a surge of interest in application of sequential deep models for diagnostic/prognostic tasks based on CT scans. Recently, a new sequential deep model based on a novel self-attention mechanism, commonly known as “Transformer” [20], has been proposed which shows superior performances in the tasks related to the sequential data. Transformer models benefit from a novel self-attention mechanism which is capable of capturing global context and dependencies between instances in a sequential data while requiring far less computational resources compared to conventional LSTM and RNN architectures. Transformers are also superior to their counterparts in terms of parallelization and dynamic attention. Although the transformer model was initially designed for Natural Language Processing, there have been recently significant attempts to adopt the self-attention mechanism for image processing applications. Vision Transformer (ViT) [21] and Convolutional Vision Transformer (CvT) [22] are two popular types of transformers designed to address image processing tasks. Both models, however, apply the self-attention to the small patches in a 2D image. Analyzing a series of CT slices, however, requires a framework capable of capturing inter-slice relations. Although development of transformers for sequential medical images is currently in its nascent stage, recent models proposed for COVID-19 disease identification and image segmentation [23, 24, 25] have shown promising results and potentials.

Contributions: In this study, we have developed an automated predictive framework based on the novel self-attention mechanism and transformer encoder, referred to as the “CAE-Transformer”. Unlike ViT and CvT, our proposed framework uses a Convolutional Auto-Encoder (CAE) model [26] to extract informative features from CT slices and stack them to form a sequential feature map. The CAE is first pre-trained on the public LIDC-IDRI dataset, then fine-tuned on our in-house dataset. The obtained sequential feature maps are then fed to a transformer model containing multiple multi-head self-attention layers, followed by a stack of fully connected layers to provide the final predictions. We also investigated the influence of Positional Embedding (PE), Global Max Pooling (GMP), and Global Average Pooling (GAP) layers, which are commonly used in transformer-based models, and realized that such layers are not as efficient as reported for models trained over a relatively small dataset like ours, and can be safely removed to build a more simplified and accurate framework. To the best of our knowledge, this study is the first one developing a transformer-based framework for lung nodule classification from volumetric non-thin CT scans.

It is also worth noting that, unlike most existing studies which

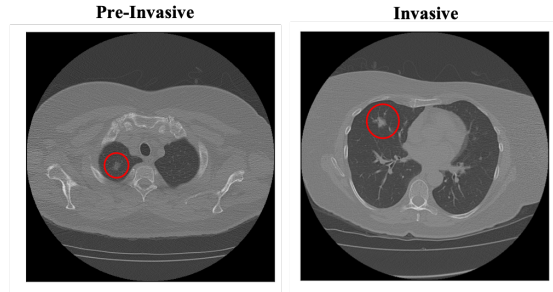


Fig. 1. Sample pre-invasive and invasive adenocarcinomas.

rely on the nodule patches as the model’s input, the CNE-Transformer does not require a detailed annotation of the nodules and takes the whole CT image as the input. The only required information from the radiologists/experts is the set of slices with the evidence of a nodule without further details. We have utilized the same dataset used in [10] with an additional five nodules from the same institution to train and evaluate the model. Experimental results showed that deep learning-based models improve the result achieved by the study performed in [10] based on the histogram-based and radiomics features while the CNE-Transformer provided the highest improvement. More specifically, the CNE-Transformer improved the accuracy from 81.0% to 87.73%, sensitivity from 80.0% to 88.67%, and specificity from 81.8% to 86.33%, while achieving the same high AUC value of 0.91.

2. CAE-TRANSFORMER FRAMEWORK

2.1. Dataset

In this study, we have used the dataset initially introduced in [10] and added five additional cases acquired from the same institution to further balance the dataset. This dataset contains volumetric CT scans of 114 pathologically proven SSNs, segmented and reviewed by 2 experienced thoracic radiologists. All SSN labels are provided after surgical resections. SSNs are initially classified into three categories of pre-invasive lesions including atypical adenomatous hyperplasia (AAH) and adenocarcinoma in situ (AIS), minimally invasive (MIA), and invasive pulmonary adenocarcinoma (IPA). Following the original study [10], we have grouped the first two categories to represent the pre-invasive and minimally invasive class with 58 cases, and kept the invasive nodules as the other class including 56 cases. In addition to the nodule labels, the CT slices with the evidence of a nodule are also specified by the radiologists, facilitating the development deep learning-based frameworks. Figure 1 shows two sample lung adenocarcinomas from the dataset.

2.2. Lung Segmentation

As the pre-processing step, we have utilized a well-trained U-Net-based lung segmentation model, introduced in [27], to extract the lung parenchyma from the CT scans. This approach has been proven beneficial to enhance the learning process and final results of the deep learning-based models in previous CT-related studies [16, 28, 29], by removing distracting components from the CT images. The extracted lung areas are then down-sampled from (512, 512) to (256, 256) to reduce the complexity and memory allocation without significant loss of information.

2.3. Convolutional Auto-Encoder (CAE)

In order to represent CT images with compressed and informative feature maps, to be used as the input of the subsequent modules, we initially pre-trained a Convolutional Auto-Encoder (CAE) based on the public LIDC-IDRI dataset, which contains 244, 527 CT images with or without the evidence of a nodule. The CAE model consists of an encoder and a decoder part. The encoder is responsible for generating a compressed representation of the input image through a stack of 5 convolution and 5 max-pooling layers followed by a fully-connected layer with the size of 256, while the decoder part attempts to reconstruct the original image using the compressed feature representation generated by the encoder. By minimizing the MSE error between the original and the reconstructed image, the CAE learns to produce highly informative feature representations for the input images. Finally, the pre-trained model is fine-tuned on in-house dataset.

2.4. Multi-Head Self-Attention Mechanism

The transformer model is the building block of the CAE-Transformer framework which uses a novel self-attention mechanism to capture global dependencies among various instances in the input sequence with a high parallelization capability, reducing the computational complexity and memory allocation of other recurrent-based architectures such as RNN and LSTM. The self-attention mechanism is based on a Scaled Dot-Product Attention function, mapping a query and a set of key-value pairs to an output, where the query (Q), keys (K), values (V), are learnable representative vectors for the instances in the input sequence with dimensions d_k , d_k , and d_v , respectively. The output of a self-attention module is computed as a weighted average of the values, where the weight assigned to each value is computed by a similarity function of the query and the corresponding key after applying a softmax function [20]. More specifically, the attention values on a set of queries are computed simultaneously, packed together into a matrix Q . The keys and values are similarly represented by matrices K and V . The output of the attention Scaled Dot-Product Attention function is computed as

$$Attention(Q, K, V) = softmax\left(\frac{QK^T}{\sqrt{d_k}}\right)V \quad (1)$$

where K^T is the transpose of the matrix K . It is also beneficial to linearly project the queries, keys, and values h times with various learnable linear projections to vectors with d_k , d_k and d_v dimensions, respectively, before applying the attention function. On each of the projected versions of queries, keys, and values, the attention function is performed in parallel, resulting in $d_v - dimensional$ output values. These values are then concatenated and once again linearly projected via a fully-connected layer. This process is called ‘‘Multi-Head Attention (MHA)’’ which helps the model to jointly attend to information from different representation subspaces at different positions [20]. The output of the MHA module is

$$MHA(Q, K, V) = Concat(head_1, \dots, head_h)W^O, \quad (2)$$

$$head_i = Attention(QW_i^Q, KW_i^K, VW_i^V),$$

where the projections are achieved by parameter matrices $W_i^Q \in \mathbb{R}^{d_{model} \times d_k}$, $W_i^K \in \mathbb{R}^{d_{model} \times d_k}$, $W_i^V \in \mathbb{R}^{d_{model} \times d_v}$, and $W^O \in \mathbb{R}^{hd_v \times d_{model}}$.

2.5. CAE-Transformer

The transformer model used in the CAE-Transformer framework is adopted from the transformer encoder proposed in [20, 21] and mod-

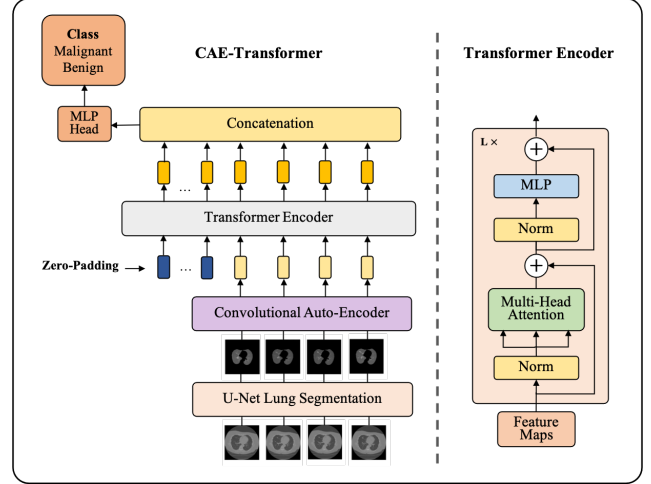


Fig. 2. Left: Pipeline of the CAE-Transformer, Right: Architecture of the Transformer Encoder

ified for the task at hand. Figure 2 illustrated the pipeline of the CAE-Transformer framework, along with the architecture of a transformer encoder. More specifically, a transformer encoder is initialized by applying the MHA on the normalized CAE-generated feature maps corresponding to input instances (i.e., CT slices), followed by a residual connection which adds low-level features of the input to the output of the MHA module. A layer normalization (LN) is then applied to the results. The normalized values are then passed to the next module which contains a Multi-Layer Perceptron (MLP), followed by another residual connection as shown in Figure 2. The CAE-Transformer is constructed by stacking 3 transformer encoder blocks on top of each other with projection, key, and query dimensions of 256, and 5 number of heads in each MHA module. Finally, the features obtained by the stack of transformer encoders from all input instances (slices) are concatenated and two Fully-Connected (FC) layers with 32 and 2 neurons, respectively, are applied to generate the final binary classification results. The last fully-connected layer uses a softmax activation function to produce probability scores. Dropout layers are incorporated to prevent the model from getting over-fitted.

It is also worth mentioning that in conventional transformers and their modified versions (e.g., ViT and CvT), some information about the position of instances in the input sequence (e.g., relative or absolute positions) are added into the model in different forms such as Positional Embeddings (PE) or Token Embeddings (TE). In subsequent sections, we have discussed that such additional information is not required in this study. As such, they have been excluded in the proposed ‘‘CNE-Transformer’’ framework, resulting in a more simplified and accurate framework. In addition, as the number of slices with the evidence of a nodule varies between different subjects (from 2 to 25 slices per nodule), we have taken the maximum number of slices in our dataset (i.e., 25 slices) and zero-padded the input sequences based on this number, so that all sequences have the same dimension of (25, 256). Furthermore, unlike existing transformers, we have not used a global pooling layer to aggregate the feature maps obtained by the last transformer encoder. Instead, we concatenated all the sequential features generated by the last transformer encoder and fed the result to the subsequent FC model to provide the final outcome. The following equations describe how

Table 1. Results obtained by the CAE-Transformer and its counterparts.

Model	Accuracy (%)	Sensitivity (%)	Specificity (%)	AUC
Ref. [10]	81.00	80.00	81.80	0.91
GMP-FC	84.02	87.00	80.67	0.90
GAP-FC	83.18	85.33	80.67	0.90
CAE-LSTM	84.92	85.00	84.33	0.84
CAE-Transformer (GMP)	77.12	83.66	71.33	0.83
CAE-Transformer (GAP)	72.65	76.33	69.33	0.80
CAE-Transformer (PE)	82.50	83.66	81.33	0.87
CAE-Transformer	87.73	88.67	86.33	0.91

the CAE-Transformer’s output is obtained as

$$\begin{aligned}
(s_1', s_2', \dots, s_{c_i}') &= U\text{-Net}(s_1, s_2, \dots, s_{c_i}), & i &= 1 \dots N \\
(f_1, f_2, \dots, f_{c_i}) &= \text{CAE}((s_1', s_2', \dots, s_{c_i}')), & i &= 1 \dots N \\
z_0 &= \text{ZeroPad}(f_1, f_2, \dots, f_{c_i}), & i &= 1 \dots N \\
z_l' &= \text{MSA}(\text{LN}(z_{l-1})) + z_{l-1}, & l &= 1 \dots L \\
z_l &= \text{MLP}(\text{LN}(z_l')) + z_l', & l &= 1 \dots L \\
o &= \text{LN}(z_L), \\
x &= [o_1, o_2, \dots, o_{25}], \\
y &= \text{MLP}(x), & & (3)
\end{aligned}$$

where s denotes the original CT slices, s' represents the segmented CT images, c_i signifies the number of slices with the evidence of a nodule in the case i , f represents the CAE-generated feature maps corresponding to the CT images, MSA denotes the Multi-Head Self-Attention module, and l shows the l_{th} MSA layer. The number 25 indicates the maximum number of slices with the evidence of a nodule per subject in this study, and y is the final prediction.

3. RESULTS

We evaluated the performance of the proposed CAE-Transformer framework using the 10-fold cross-validation method. The CAE model is pre-trained using a batch size of 128, learning rate of $1e-4$ and 200 epochs. The best model on the randomly sampled 20% of the dataset was selected as the best model. The model was then fine-tuned on the in-house dataset using a lower learning rate of $1e-6$ and 50 epochs. To fine tune the final CAE, only the middle fully-connected layer and its previous and next convolution layers were trained while the other layers have been kept unchanged. The CAE-generated features were then used to train the transformer encoder. The transformer was trained using a learning rate of $1e-4$, batch size of 64, and 200 epochs. The results of the CAE-Transformer are presented in Table 1.

We have compared the performance of the proposed CAE-Transformer framework with the results obtained by the model proposed in [10]. As the other models proposed in the literature are not trained over the same dataset, they are not considered for comparison. We have further compared the CAE-Transformer with non-transformer alternative models by aggregating the CAE-generated feature maps using GMP and GAP, followed by a stack of fully connected and batch normalization layers. The best experimental results for such models were obtained by utilizing 4 fully connected layers with 128, 128, 32, and 2 neurons, respectively. We have also compared the performance of the CAE-Transformer with its LSTM-based counterpart, referred to as the ‘‘CAE-LSTM’’,

obtained by replacing the transformer blocks with a stack of LSTM layers while using the same hyper-parameters and complexity. In another experiment, we have replaced the final concatenation layer in the CAE-Transformer with GMP and GAP to evaluate their influence on the model while the rest of the model remained the same. More specifically, in separate experiments, we have used GMP and GAP to aggregate the sequential feature maps generated by the last transformer encoder instead of considering the entire features using concatenation. As the last experiment, we have incorporated the PE to investigate its influences on the model.

The experimental results provided in Table 1 shows that most deep learning-based models outperform the original radiomics and machine learning-based model, while the proposed CAE-Transformer achieves the best performance among the developed frameworks. The results also demonstrate that incorporating the GAP, GMP, and PE into the model deteriorates the performance in our study. In the case of PE, we suspect that understanding additional positional relations can be challenging when the model is trained on a relatively small dataset like ours. The recently published study in [30] also reports the same issue when a small training dataset is used to train a transformer. It is worthy of note that increasing the complexity of the model could improve the performance when GAP, GMP, and PE were included. The improvements, however, were minor and could not reach the CAE-Transformer’s results.

4. CONCLUSION

In conclusion, we have developed an automated transformer-based framework, referred to as the ‘‘CAE-Transformer’’, to enhance the existing radiomics and machine learning-based models aiming to predict the invasiveness of lung adenocarcinoma subsolid nodules from 3D CT scans. The proposed CAE-Transformer framework significantly improved the performance of the previously developed models by increasing the accuracy by 6.73%, sensitivity by 8.67%, and specificity by 84.53%. The CAE-Transformer is also capable of capturing global inter-slice relations in a volumetric CT scan while requiring less computational resources compared to RNN and LSTM. We have also investigated the effects of GMP, GAP, and PE in our model and realized that such components of a conventional transformer are not beneficial for the task at hand, especially in our case that the training dataset is relatively small. As future works, we will be collaborating with our partners in medical centers to increase the size and diversity of the dataset and target the three-way SSN classification task. Furthermore, we would like to investigate the effects of embedding the radiomics and morphological features in the CAE-Transformer framework.

5. REFERENCES

- [1] S.D. Kamath, S.M. Kircher, and A.B. Benson, "Comparison of Cancer Burden and Nonprofit Organization Funding Reveals Disparities in Funding Across Cancer Types," *Journal of the National Comprehensive Cancer Network*, vol. 17, no. 7, pp. 849–854, jul 2019.
- [2] F. Bray et al., "Global cancer statistics 2018: GLOBOCAN estimates of incidence and mortality worldwide for 36 cancers in 185 countries," *CA: A Cancer Journal for Clinicians*, vol. 68, no. 6, pp. 394–424, nov 2018.
- [3] R.S. Herbst, D. Morgensztern, and C. Boshoff, "The biology and management of non-small cell lung cancer," *Nature*, vol. 553, no. 7689, pp. 446–454, jan 2018.
- [4] H.Y. Kim, Y.M. Shim, K.S. Lee, J. Han, C.A. Yi, and Y.K. Kim, "Persistent Pulmonary Nodular Ground-Glass Opacity at Thin-Section CT: Histopathologic Comparisons," *Radiology*, vol. 245, no. 1, pp. 267–275, oct 2007.
- [5] J. Lai, Q. Li, F. Fu, Y. Zhang, Y. Li, Q. Liu, and H. Chen, "Subsolid Lung Adenocarcinomas: Radiological, Clinical and Pathological Features and Outcomes," *Seminars in Thoracic and Cardiovascular Surgery*, jun 2021.
- [6] X. Cui et al., "A Subsolid Nodules Imaging Reporting System (SSN-IRS) for Classifying 3 Subtypes of Pulmonary Adenocarcinoma," *Clinical Lung Cancer*, vol. 21, no. 4, pp. 314–325.e4, jul 2020.
- [7] X. Shao, R. Niu, Z. Jiang, X. Shao, and Y. Wang, "Role of PET/CT in Management of Early Lung Adenocarcinoma," *American Journal of Roentgenology*, vol. 214, no. 2, pp. 437–445, feb 2020.
- [8] E.A. Kazerooni and otehrs, "ACR–STR Practice Parameter for the Performance and Reporting of Lung Cancer Screening Thoracic Computed Tomography (CT)," *Journal of Thoracic Imaging*, vol. 29, no. 5, pp. 310–316, sep 2014.
- [9] K. Fujii, K. McMillan, M. Bostani, C. Cagnon, and M. McNitt-Gray, "Patient Size–Specific Analysis of Dose Indexes From CT Lung Cancer Screening," *American Journal of Roentgenology*, vol. 208, no. 1, pp. 144–149, jan 2017.
- [10] A. Oikonomou and otehrs, "Histogram-based models on non-thin section chest CT predict invasiveness of primary lung adenocarcinoma subsolid nodules," *Scientific Reports*, vol. 9, no. 1, pp. 6009, dec 2019.
- [11] D. Gu, G. Liu, and Z. Xue, "On the performance of lung nodule detection, segmentation and classification," *Computerized Medical Imaging and Graphics*, vol. 89, pp. 101886, apr 2021.
- [12] C. Gao, P. Xiang, J. Ye, P. Pang, S. Wang, and M. Xu, "Can texture features improve the differentiation of infiltrative lung adenocarcinoma appearing as ground glass nodules in contrast-enhanced CT?," *European Journal of Radiology*, vol. 117, pp. 126–131, aug 2019.
- [13] J. Uthoff et al., "Machine learning approach for distinguishing malignant and benign lung nodules utilizing standardized perinodular parenchymal features from CT," *Medical Physics*, vol. 46, no. 7, pp. 3207–3216, jul 2019.
- [14] G. Kang, K. Liu, B. Hou, and N. Zhang, "3D multi-view convolutional neural networks for lung nodule classification," *PLOS ONE*, vol. 12, no. 11, pp. e0188290, nov 2017.
- [15] S. Liu, Y. Xie, A. Jirapatnakul, and A.P. Reeves, "Pulmonary nodule classification in lung cancer screening with three-dimensional convolutional neural networks," *Journal of Medical Imaging*, vol. 4, no. 04, pp. 1, nov 2017.
- [16] S. Heidarian et al., "COVID-FACT: A Fully-Automated Capsule Network-Based Framework for Identification of COVID-19 Cases from Chest CT Scans," *Frontiers in Artificial Intelligence*, vol. 4, may 2021.
- [17] S. Heidarian et al., "Ct-Caps: Feature Extraction-Based Automated Framework for Covid-19 Disease Identification From Chest Ct Scans Using Capsule Networks," in *ICASSP 2021 - 2021 IEEE International Conference on Acoustics, Speech and Signal Processing (ICASSP)*. jun 2021, pp. 1040–1044, IEEE.
- [18] M.M. Farhangi, N. Petrick, B. Sahiner, H. Frigui, A.A. Amini, and A. Pezeshk, "Recurrent attention network for false positive reduction in the detection of pulmonary nodules in thoracic CT scans," *Medical Physics*, vol. 47, no. 5, pp. 2150–2160, may 2020.
- [19] S.G. Armato et al., "The Lung Image Database Consortium (LIDC) and Image Database Resource Initiative (IDRI): A Completed Reference Database of Lung Nodules on CT Scans," *Medical Physics*, vol. 38, no. 2, pp. 915–931, jan 2011.
- [20] A. Vaswani et al., "Attention is all you need," in *Advances in Neural Information Processing Systems*, I. Guyon, U. V. Luxburg, S. Bengio, H. Wallach, R. Fergus, S. Vishwanathan, and R. Garnett, Eds. 2017, vol. 30, Curran Associates, Inc.
- [21] A. Dosovitskiy et al., "An Image is Worth 16x16 Words: Transformers for Image Recognition at Scale," oct 2020.
- [22] H. Wu, B. Xiao, N. Codella, M. Liu, X. Dai, L. Yuan, and L. Zhang, "CvT: Introducing Convolutions to Vision Transformers," mar 2021.
- [23] X. Gao, Y. Qian, and A. Gao, "COVID-VIT: Classification of COVID-19 from CT chest images based on vision transformer models," jul 2021.
- [24] A.A.E. Ambita, E.N.V. Boquiao, and P.C. Naval, "COViT-GAN: Vision Transformer for COVID-19 Detection in CT Scan Images with Self-Attention GAN for Data Augmentation," pp. 587–598. 2021.
- [25] C.C. Hsu, G.L. Chen, and M.H. Wu, "Visual Transformer with Statistical Test for COVID-19 Classification," jul 2021.
- [26] J. Masci, U. Meier, D. Cireşan, and J. Schmidhuber, "Stacked Convolutional Auto-Encoders for Hierarchical Feature Extraction," pp. 52–59. 2011.
- [27] J. Hofmanninger, F. Prayer, J. Pan, S. Röhrich, H. Prosch, and G. Langs, "Automatic lung segmentation in routine imaging is primarily a data diversity problem, not a methodology problem," *European Radiology Experimental*, vol. 4, no. 1, pp. 50, dec 2020.
- [28] P. Afshar et al., "Human-level COVID-19 Diagnosis from Low-dose CT Scans Using a Two-stage Time-distributed Capsule Network," may 2021.
- [29] A. Mohammadi et al., "Diagnosis/Prognosis of COVID-19 Chest Images via Machine Learning and Hypersignal Processing: Challenges, opportunities, and applications," *IEEE Signal Processing Magazine*, vol. 38, no. 5, pp. 37–66, sep 2021.
- [30] J.M.J. Valanarasu, P. Oza, I. Hacihaliloglu, and V.M. Patel, "Medical Transformer: Gated Axial-Attention for Medical Image Segmentation," pp. 36–46. 2021.